# Box6D: Zero-shot Category-level 6D Pose Estimation of Warehouse Boxes

Yintao Ma, Sajjad Pakdamansavoji, Amir Rasouli, Tongtong Cao Huawei Technologies Canada

### **Abstract**

Accurate and efficient 6D pose estimation of novel objects under clutter and occlusion is critical for robotic manipulation across warehouse automation, bin picking, logistics, and e-commerce fulfillment. There are three main approaches in this domain; Model-based methods assume an exact CAD model at inference but require high-resolution meshes and transfer poorly to new environments; Modelfree methods that rely on a few reference images or videos are more flexible, however often fail under challenging conditions; Category-level approaches aim to balance flexibility and accuracy but many are overly general and ignore environment and object priors, limiting their practicality in industrial settings.

To this end, we propose **Box6D**, a category-level 6D pose estimation method tailored for storage boxes in the warehouse context. From a single RGB-D observation, Box6D infers the dimensions of the boxes via a fast binary search and estimates poses using a category CAD template rather than instance-specific models. Suing a depth-based plausibility filter and early-stopping strategy, Box6D then rejects implausible hypotheses, lowering computational cost. We conduct evaluations on real-world storage scenarios and public benchmarks, and show that our approach delivers competitive or superior 6D pose precision while reducing inference time by approximately 76%.

# 1. Introduction

Robotic systems are increasingly deployed in modern warehouses and distribution centers, making autonomous logistics a central research focus. To be effective, these systems should be able to accurately and efficiently estimate 6D poses (3D position and 3D orientation) of *novel* objects in order to perform fundamental manipulation tasks, such as picking, placing, and transporting.

6D pose estimation approaches are dominantly modelbased. They assume a high-resolution instance-level CAD model for each target and rely on extensive template rendering at inference. This requirement limits scalability and transfer to new environments. To remedy this prob-

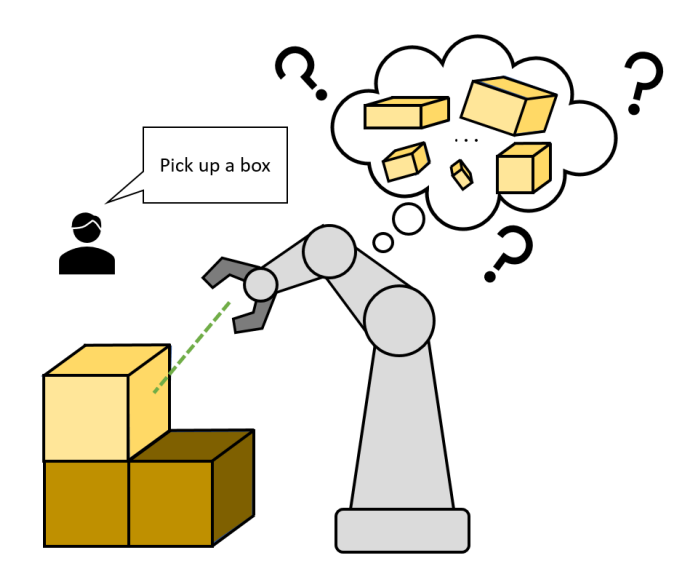


Figure 1. A typical storage scenario in which the robot is tasked with picking up a box. The green line highlights the target box to be manipulated. Before grasping, the robot must accurately predict the pose and scale of the observed box.

lem, model-free and category-level methods have been proposed. The former only uses a few reference frames or videos and the latter uses a generic CAD template per category. These approaches, however, are not suitable for warehouse settings where objects are packed in boxes of various dimensions and appearances. On one hand, maintaining instance-level CAD libraries for such inventories could be very costly. Model-free models would also struggle to accurately estimate poses due to symmetric geometry of boxes and their lack of distinctive visual features [7]. On the other hand, existing approaches fail to leverage strong contextual priors, such as common object types and structured storage layouts, reducing their robustness to clutter and occlusion.

We address these gaps by proposing a zero-shot category-level 6D pose estimation pipeline tailored for boxes in warehouse settings. Specifically, we extend SAM6D–a *model-based* method–to operate with a single category-level CAD template by adding a dimension-estimation module that infers box sizes from a single RGB-D observation. To improve robustness to symmetry and geometric ambiguity, we incorporate a depth-based plau-

sibility filter that rejects inconsistent pose hypotheses. At the end, we incorporate an early-stopping strategy to reduce computation without sacrificing accuracy.

In summary, the contributions of this work are:

- We propose a novel zero-shot model-based 6D pose estimator for warehouse settings. Our method effectively estimates poses of symmetric objects using depth consistent filtering and benefits from an early stopping mechanism, which significantly minimize computation time, making an ideal solution for real-time applications
- We conduct extensive evaluation on public benchmark datasets and our in-house data collected in a warehouse to showcase the benefits of our approach compared to stateof-the-art algorithms.
- We conduct ablation studies to highlight the benefits of the proposed modules on the overall performance of our model.

#### 2. Related Works

The focus of this work is on 6D pose estimation of *unseen* symmetric/box-shaped objects in warehouse settings. The approaches that can be used for this purpose can be categorized based on their reliance on CAD models.

*Model-based* methods achieve high accuracy by exploiting a known 3D model at inference, typically as 2D–2D render-and-search that matches rendered views to the input image [2], as 2D–3D correspondence pipelines that extract keypoints and solve with RANSAC/PnP [18], or as 3D–3D point-cloud alignment that estimates the rigid transform via an SVD solver [9]. However, these pipelines require high-quality, instance-level meshes and large template banks; building and maintaining them at scale is costly and brittle, which limits transfer to new environments and hinders large warehouse deployments.

*Model-free* methods remove the need for CAD models altogether. Some learn generalizable priors that map images directly to pose or to intermediate object-centric coordinates [17]. Others adopt one-shot or few-shot regimes that construct an implicit reference from a small set of images or short videos of the novel object [1, 10, 15, 19]. While this flexibility is appealing, warehouse objects often exhibit symmetries, geometric ambiguity, weak or repetitive texture, and clutter. Under these conditions, feature matching becomes unreliable and accuracy degrades, especially when real-time constraints and occlusion are present.

Category-level methods aim to balance accuracy and mesh dependence by using a generic CAD template per category rather than an instance mesh. This reduces the maintenance burden while retaining useful geometric structure. In practice, though, many category-level approaches are designed to be broadly applicable and do not leverage domain-specific priors that are common in industrial settings [6, 21]. They typically ignore strong object priors (e.g. focusing

only on boxes) and environmental regularities (such as typical storage layouts in warehouses), which limits their robustness under symmetry, geometric confusion, and scarce appearance cues. In this work, we adopt a category-level approach tailored to 6D pose estimation of boxes in warehouse settings.

### 3. Method

Our proposed framework, Box6D, consists of five components: **Object detection**, which localizes the target and produces a segmentation mask; **Pose estimation**, which generates multiple pose hypotheses via point-cloud matching; **Depth-consistency filter**, which rejects hypotheses whose rendered depths are inconsistent with the observed depth; **Dimension estimation**, which iteratively estimates the box dimensions along the X, Y, and Z axes; and **Early stopping**, which terminates the pipeline upon convergence. An overview of the framework is shown in Fig. 2. Details of each module are provided below.

## 3.1. Object detection

Following SAM6D's Instance Segmentation Model (ISM) [13], we prompt SAM [8] to produce class-agnostic mask proposals on the observed image, filter them by confidence and non-maximum suppression (NMS), and then apply an object-matching score to keep only proposals consistent with the target instance [8, 13]. The matching combines high-level semantics with coarse geometric consistency, without requiring per-class training [13, 16]. The retained proposals provide the bounding boxes and segmentation masks passed to the pose estimation stage [13].

#### 3.2. Pose estimation

We estimate pose via 3D–3D correspondences between the observation and the generic category model point clouds. Following SAM6D [13], a lightweight proposal network produces multiple initial pose hypotheses. We then apply simple depth-consistence validity check to prune implausible hypotheses. From the remaining set, we select the highest-confidence hypothesis and feed it to a refinement network that further aligns the point clouds to sharpen rotation and translation estimations.

### 3.3. Depth-consistency filter

Boxes are often symmetric along several axes and their textures are weak or repetitive. As a result, hypotheses with incorrect rotations can obtain confidence scores that are similar to correct ones in the pose-proposal stage. A wrong rotation typically swaps the visible face with an opposite face, which makes the rendered geometry inconsistent with the observed depth. This ambiguity is common for stacked boxes where coarse poses can appear to "hover" above the

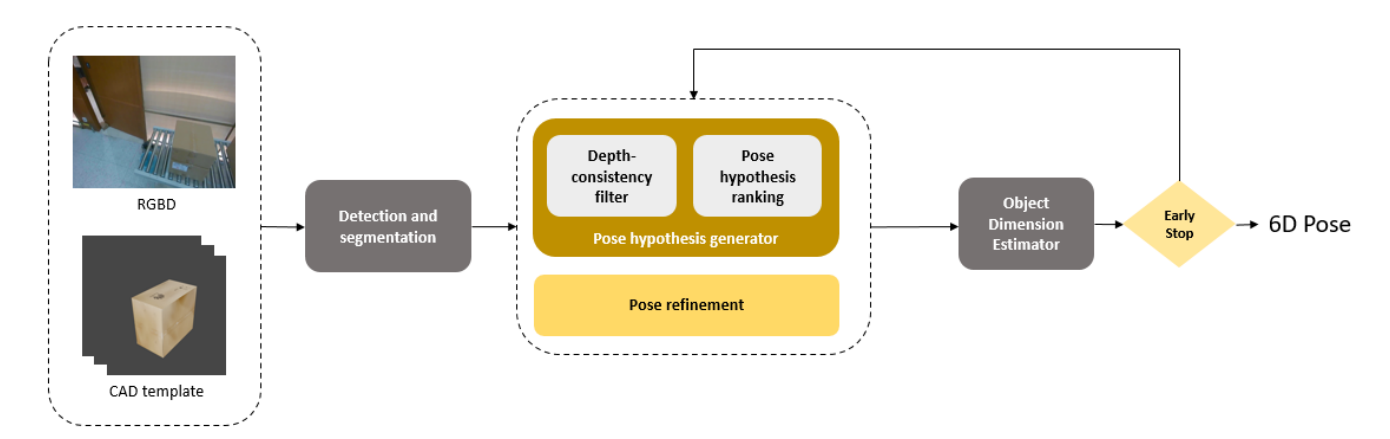


Figure 2. Overview of the Box6D pipeline. The observed RGB–D image and a rendered RGB–D category box template are first used for detection and segmentation. The detections are passed to the pose estimator to generate multiple pose hypotheses, reject those with depth inconsistency, and refine the high-confidence candidates. The resulting pose guides dimension estimation by comparing the projected CAD mask to the observation; the CAD is rescaled accordingly and fed back to pose estimation. This project–compare–rescale loop repeats until convergence or terminates early via the early-stopping module.

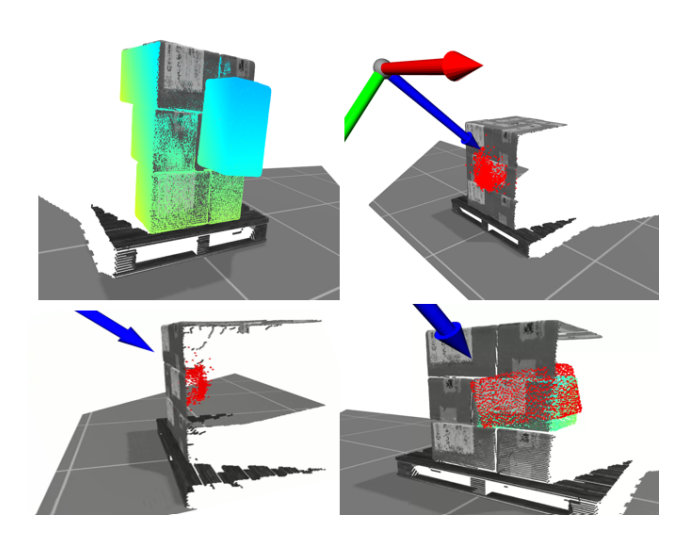


Figure 3. An example of how depth-consistency filter improves 6D pose precision. (**Top left**): A rejected pose hypothesis produces inconsistent depth, protruding from the stack of boxes. (**Top right**): Centers of all pose hypotheses, shown as red points; those with inconsistent depth lie outside the box stack. (**Bottom left**): Centers of the remaining pose hypotheses after the depth-consistency filter, shown as red points; the centers now lie within the box stack. (**Bottom right**): Correct 6D pose estimated after applying the depth-consistency filter. Estimated pose is marked with red and ground-truth is marked with green.

true surface (see Fig. 3). We address it with a simple depthconsistency filter: for each hypothesis, we render the model into the camera frame and compare its depth with the observed depth inside the predicted mask. Hypotheses that violate depth consistency are discarded. The remaining set preserves the correct high-confidence solution and enables a more reliable refinement stage.

### 3.4. Dimension estimation

We estimate box dimensions by starting from a canonical, category level CAD template and the 6D pose recovered by our pose estimation module. With this pose fixed for the current iteration, we scale the CAD independently along the X, Y, and Z axes, place the scaled model at the estimated pose, and project its vertices into the camera using the known intrinsics to create a synthetic mask. We then compare this CAD mask with the observed object mask by measuring their axis aligned pixel extents along the image directions that correspond to the three box axes.

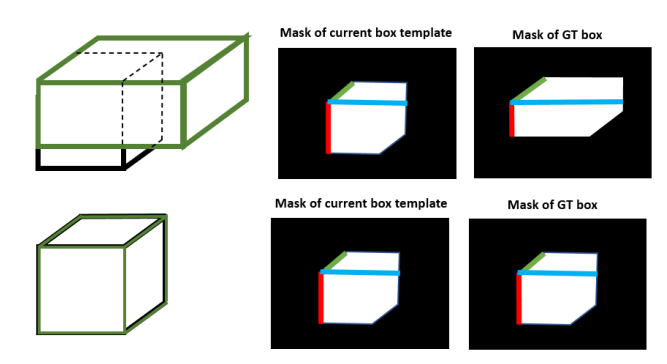


Figure 4. An example of scaling the template box to align with the target box. (**Top):** The template box (green) is mismatched in scale with the target box (black). We compare the observed mask of the target and the projected mask of the template along all axes using their pixel extents, indicated by red, green, and blue lines. (**Bottom):** After iterative comparison, rescaling, and pose refresh, convergence is reached: the mask extents along all axes fall within a specified threshold, and the scale is correctly estimated.

For each axis, the comparison gives a binary decision:

if the CAD underfills the observation we increase the scale on that axis, and if it overfills we decrease it (Fig. 4). We implement this as a binary search over scale on each axis, updating the lower or upper bound based on the decision and setting the next hypothesis to the midpoint of the interval. After each scale update, we refresh the 6D pose using the updated CAD so that coupling between scale and pose does not accumulate and the alignment remains stable.

The process repeats, projects, compares, decides, updates bounds, and reestimates the pose, until a convergence criterion is met. The criterion, for example, can eb one of the following, small per axis extent error (eg. 10 pixels), sufficiently tight search intervals, or reaching a maximum number of iterations. See Algorithm 1.

### Algorithm 1 Binary Search for Box Dimensions

```
Require: Canonical CAD \mathcal{C}, intrinsics K, observed mask
      \mathcal{M}_{\text{obs}}, initial pose T_0, per-axis bounds \ell, u, tolerances
      \tau_{\rm px}, \tau_{\rm scale}, \, {\rm max \, iters} \, T_{\rm max}
```

```
Ensure: Scales s and pose T
  1: s \leftarrow (1, 1, 1); \quad T \leftarrow T_0
  2: for t = 1 to T_{\text{max}} do
           T \leftarrow \mathsf{POSEESTIMATE}(\mathcal{C}(s))
           \mathcal{M}_{\text{cad}} \leftarrow \text{RenderMask}(\mathcal{C}(s), T, K)
  4:
           e_{\text{cad}} \leftarrow \text{EXTENTS}(\mathcal{M}_{\text{cad}})
  5:
           e_{\text{obs}} \leftarrow \text{EXTENTS}(\mathcal{M}_{\text{obs}})
  6:
           if \max_a |e_{\operatorname{cad},a} - e_{\operatorname{obs},a}| \le \tau_{\operatorname{px}} then
  7:
               break
  8:
  9:
           end if
 10:
           m \leftarrow e_{\text{obs}} - e_{\text{cad}}
           update bounds elementwise: \ell_a \leftarrow s_a if m_a > 0;
 11:
           otherwise u_a \leftarrow s_a
           s \leftarrow (\ell + u)/2
 12:
13: end for
14: return s, T
```

### 3.5. Early stopping

Once rotation has stabilized and the projected box axes are aligned around the CAD vertex, the remaining uncertainty is scaled only, so we replace iterative search with a one step proportional update. We measure the axis aligned pixel extents of the observed mask and the current CAD mask, take their per-axis ratios, and scale the CAD accordingly in a single update. A brief search is still necessary at the beginning because the pose estimator is sensitive to scale and needs a roughly correct template size to lock onto the right orientation. After that initial phase, the proportional update serves as a closed form solution for the final dimensions as shown in Fig. 5. In practice, we apply the proportional scaling, refresh the pose once to absorb any residual coupling between scale and pose, and stop, which removes unnecessary binary search iterations and cuts computation time substantially (

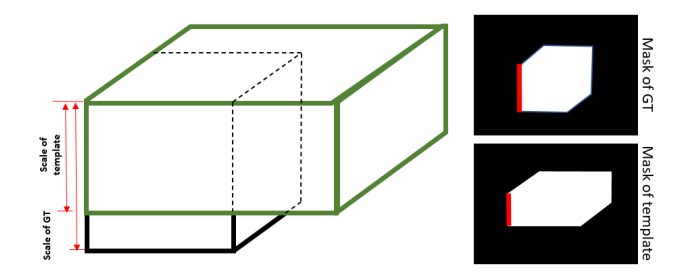


Figure 5. An example of estimating the target box scale using a closed-form update when the early-stopping criterion is satisfied. (Left:) The template box (green) and target box (black) poses are aligned at a vertex, and the only remaining difference is scale. The scale mismatch is indicated by red lines. (Right:) The same scale difference is visualized on the observed and projected masks of the target and template boxes with red lines. The ratio of these red-line extents is used to solve for the scale.

### Algorithm 2 Early stopping via proportional scaling

```
Require: Canonical CAD \mathcal{C}, intrinsics K, observed mask
     \mathcal{M}_{obs}, current pose T, current scales s
```

**Ensure:** Final scales s, pose T

```
1: if AXESALIGNEDAROUNDVERTEX(C(s), T) then
         \mathcal{M}_{\text{cad}} \leftarrow \text{RENDERMASK}(\mathcal{C}(s), T, K)
          e_{\text{cad}} \leftarrow \text{EXTENTS}(\mathcal{M}_{\text{cad}})
 3:
          e_{\text{obs}} \leftarrow \text{EXTENTS}(\mathcal{M}_{\text{obs}})
 4:
 5:
         r \leftarrow \text{RATIO}(e_{\text{obs}}, e_{\text{cad}})
 6:
          s \leftarrow \text{RESCALE}(s, r)
 7:
         T \leftarrow \text{PoseEstimate}(\mathcal{C}(s))
         return s, T
 8:
 9: else
         return BINARY SEARCH REFINE (C, K, \mathcal{M}_{obs}, T, s)
10:
11: end if
```

Alg. 2).

### 4. Experiments

Datasets. We evaluate our method on three datasets that together span dense clutter, multiple instances, static and dynamic scenes, tabletop and robotic manipulation settings, and objects that are often textureless, reflective, symmetric, and varied in size.

A proprietary in-house RGB-D collection captured in a warehouse and tabletop setups with diverse lighting, background clutter, and occlusion. This data contains multi-view sequences with multiple box instances per scene and motion from both camera and objects.

HouseCat6D comprises real and synthetic RGB-D data of household scenes with significant clutter and frequent occlusions. It includes multi-instance arrangements and varied surface properties, including low texture and specular reflections. We evaluate on the box-like subset relevant to our category-level setting, using 4 scenes with 2229 object instances.

PACE focuses on manipulation-centric scenes, with tabletop layouts and robot interactions that induce both static and dynamic occlusion patterns. The dataset covers challenging geometries and materials, including symmetric and reflective objects. We use the packaging/box subset for category-level evaluation, comprising 63 test scenes and 11638 object instances.

Across these three sources, the combination of cluttered household environments, warehouse-style layouts, and manipulation scenarios provides a varied and demanding benchmark for category-level 6D pose and dimension estimation, enabling a thorough assessment of accuracy and robustness.

**Metrics.** Following prior work [20], we report 3D Intersection-over-Union (IoU) at thresholds of 25% and 50%. We also measure pose accuracy using an  $n^{\circ}/m$ ,cm criterion: a prediction counts as a true positive only if its rotation error is at most  $n^{\circ}$  and its translation error is at most m,cm.

**Models.** In our evaluations, we primarily compare Box6D against SAM6D. For the public benchmarks, we follow the respective leaderboards: on HouseCat6D we compare with NOCS[20], FS-Net[4], GPV-Pose[5], VI-Net[12], AG-Pose[14], and SecondPose[6]; on PACE we compare with NOCS[20], HS-Pose[22], SGPA[3], SAR-Net[11], and CPPF++[21].

### 4.1. 6D Pose Estimation on Warehouse datasets

We compare our method on the warehouse data against two baselines: SAM6D with a fixed category template and SAM6D with ground-truth meshes. As shown in Table 1, the fixed template performs poorly at strict overlap thresholds (precision 0.06 at IoU = 0.5, 0.02 at IoU = 0.7, and 0.00 at IoU = 0.9), while Box6D attains perfect precision at IoU = 0.5 and 0.7 and reaches 0.92 at IoU = 0.9, closely approaching the GT CAD oracle at 0.95. This small gap indicates that our dimension refinement accurately recovers instance scale and preserves high-precision pose without access to per-instance meshes. Further qualitative comparison is given in Fig. 7.

### 4.2. 6D Pose Estimation on HouseCat6D

We evaluate on HouseCat6D using the leaderboard's category-level metrics (IoU at 25% and 50%) and compare our box results against published state-of-the-art models. As shown in Table 2, Box6D attains the highest scores at both thresholds, reaching 88.8 at IoU = 0.25 and 58.9 at IoU = 0.50. This substantially exceeds the next best method

Table 1. Comparison of Box6D and baselines on the proprietary warehouse dataset. 6D pose performance is reported as average precision at IoU = 0.50, 0.70, and 0.90.

Model	loU=.5	IoU=.7	IoU=.9
SAM6D + box's CAD template	0.06	0.02	0.00
SAM6D + GT CAD	1.00	1.00	0.95
Box6D (Ours)	1.00	1.00	0.92









Figure 6. Qualitative comparison of Box6D with the baseline. Estimated poses are shown as red point clouds. (**Top left**): a scene from our proprietary warehouse dataset. (**Top right**): ground-truth pose. (**Bottom left**): Box6D estimate. (**Bottom right**): SAM6D estimate using the category CAD template.

(SecondPose at 54.5 and 23.7, respectively). Further qualitative comparison is given in Fig. 7.

Table 2. Comparison of Box6D with state-of-the-art models from the HouseCat6D leaderboard. 6D pose performance is reported as average precision at IoU = 0.25 and 0.50.

Model	loU=.25	IoU=.50
FS-Net	31.7	1.2
GPV-Pose	31.4	1.1
NOCS	43.3	6.5
VI-Net	44.8	12.7
SecondPose	54.5	23.7
AG-Pose	57.2	7.7
Box6D (Ours)	88.8	58.9

#### 4.3. 6D Pose Estimation on PACE

We compare our method on PACE against leading approaches using IoU at 25% and 50% and Average Precision (AP) under three pose-accuracy criteria: rotation  $\leq 20^{\circ}$ , translation  $\leq 5$  cm, and their conjunction. As shown in Table 3, Box6D achieves the best IoU scores (63.2 at IoU = 0.25 and 10.4 at IoU = 0.50) and the highest AP for rotation  $\leq 20^{\circ}$  (0.8) and for the combined  $\leq 20^{\circ}$ —5 cm crite-



Figure 7. Qualitative comparison of Box6D with AG-Pose. Estimated poses are shown as red point clouds. (**Top left):** a scene from the HouseCat6D dataset. (**Top right):** ground-truth pose. (**Bottom left):** Box6D estimate. (**Bottom right):** AG-Pose estimates.

rion (0.5), surpassing CPPF++[21] (27.2, 0.0, 0.7, and 0.4, respectively). The only exception is AP 5cm, where HS-Pose[22] ranks first at 56.5 and Box6D is a close second at 54.1. Further qualitative comparisons are provided in Fig. 8.

Table 3. Comparison of Box6D with state-of-the-art models from the PACE leaderboard. We report 6D pose performance as average precision at IoU = 0.25 and 0.50, and under three pose-accuracy criteria: rotation  $\leq 20^\circ$ , translation  $\leq 5$  cm, and their conjunction.

Model IoU=.25 IoU=.50		IoU= 50	AP		
		0:20°	5cm	0 : 20°-5cm	
NOCS	0	0	0	52.6	0
SGPA	0	0	0.1	19.8	0
HS-Pose	0.8	0	0	56.5	0
SAR-Net	1.3	0	0	46.7	0
CPPF++	27.2	0	0.7	21.2	0.4
Box6D (Ours)	63.2	10.4	0.8	54.1	0.5

### 5. Ablations

**Depth Consistency Filter.** We ablate the depth-consistency filter on the warehouse dataset by estimating 6D pose with and without this step and measure precision at IoU = 0.80. As shown in Table 4, adding the filter lifts performance from 0.53 to 0.86, an absolute gain of 0.33 and a relative improvement of about 62.3%. This confirms that rejecting hypotheses whose rendered depth is inconsistent with the observed depth substantially improves final pose

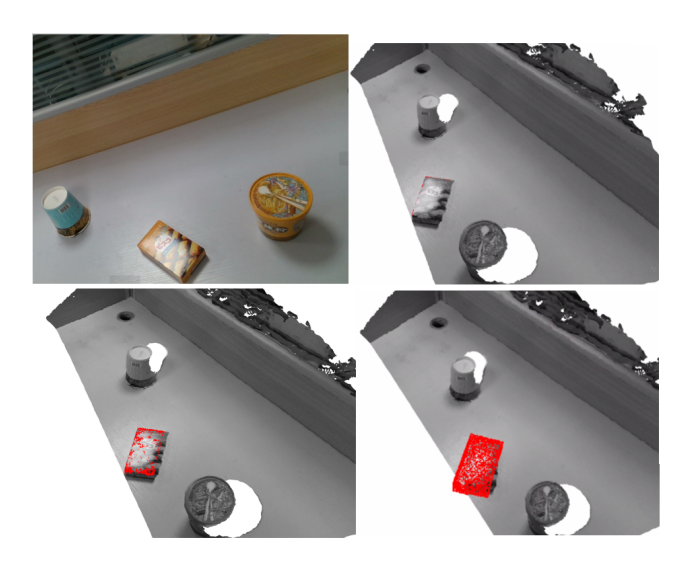


Figure 8. Qualitative comparison of Box6D with CPPF++. Estimated poses are shown as red point clouds. (**Top left**): a scene from PACE dataset. (**Top right**): ground-truth pose. (**Bottom left**): Box6D estimate. (**Bottom right**): CPPF++ estimates.

accuracy.

Table 4. Effect of the depth-consistency filter on 6D pose accuracy on the warehouse dataset. We report precision at IoU = 0.80.

Method	IoU=.80
Without Filter	0.53
Depth Consistency Filter	0.86

**Early Stopping.** We ablate the effect of adding early stopping at inference time to our pipeline on the warehouse dataset in Table 5. We measure mean wall-clock time per frame over 50 runs with and without the early-stopping stage and report 6D pose precision at IoU = 0.9. Adding early stopping reduces the average runtime from  $4.93 \pm 2.39 \text{ s}$  to  $1.16 \pm 0.74 \text{ s}$ , a 76% decrease and roughly a  $4.3 \times 1.00 \times 1.$ 

Table 5. Effect of early stopping on runtime and accuracy on the warehouse dataset. We report average precision at IoU = 0.90 and inference time averaged over 50 runs.

Method	loU=.9	Time(s)
Binary search	<b>0.94</b>	$4.93 \pm 2.39$
+ Early Stopping	0.92	$1.16 \pm 0.74$

### 6. Conclusion

We proposed Box6D, a zero-shot category-level 6D pose estimator tailored for box-shaped objects in a warehouse setting. Building on a model-based pipeline, Box6D generalizes to categories by estimating instance dimensions with an efficient binary search over per-axis scale. To handle symmetry, geometric ambiguity, and weak texture, we add a depth-consistency filter that rejects pose hypotheses whose rendered depth disagrees with the observation. We further reduce runtime by over 75% with an early-stopping module that switches to a proportional, one-step scale update once rotation is stable, without sacrificing final precision. Ablations on our proprietary warehouse data confirm the contribution of each stage, and evaluations on two public benchmarks, HouseCat6D and PACE, show that Box6D achieves state-of-the-art performance.

### References

- [1] Jan Kautz Bowen Wen, Wei Yang and Stan Birchfield. Foundationpose: Unified 6d pose estimation and tracking of novel objects. *CVPR*, 2024. 2
- [2] E. Brachmann, A. Krull, F. Michel, S. Gumhold, J. Shotton, and C. Rother. Learning 6d object pose estimation using 3d object coordinates. ECCV, 2014. 2
- [3] Kai Chen and Qi Dou. Sgpa: Structure-guided prior adaptation for category-level 6d object pose estimation. In *Proceedings of the IEEE/CVF International Conference on Computer Vision*, pages 2773–2782, 2021. 5
- [4] Wei Chen, Xi Jia, Hyung Jin Chang, Jinming Duan, Linlin Shen, and Ales Leonardis \*. Fs-net: Fast shape-based network for category-level 6d object pose estimation with decoupled rotation mechanism. CVPR, 2021. 5
- [5] Yan Di, Ruida Zhang, Zhiqiang Lou, Fabian Manhardt, Xiangyang Ji, Nassir Navab, and Federico Tombari. Gpv-pose: Category-level object pose estimation via geometry-guided point-wise voting. CVPR, 2022. 5
- [6] H. Du, Y. Li, Y. Di, T. Zhang, Y. Sun, and J. Zhu. Secondpose: Se(3)-consistent dual-stream feature fusion for category-level pose estimation. *IEEE Transactions on Instrumentation and Measurement*, 2025. 2, 5
- [7] HyunJun Jung, Guangyao Zhai, Shun-Cheng Wu, Patrick Ruhkamp, Hannah Schieber, Giulia Rizzoliand Pengyuan Wang, Hongcheng Zhao, Lorenzo Garattoni, Sven Meier, Daniel Roth, Nassir Navab, and Benjamin Busam. A largescale multi-modal category level 6d object perception dataset with household objects in realistic scenarios. CVPR, 2024. 1
- [8] Alexander Kirillov, Eric Mintun, Nikhila Ravi, Hanzi Mao, Chloe Rolland, Laura Gustafson, Tete Xiao, Spencer Whitehead, Alexander C Berg, Wan-Yen Lo, et al. Segment anything. In *Proceedings of the IEEE/CVF international confer*ence on computer vision, pages 4015–4026, 2023. 2
- [9] Yann Labbé, Lucas Manuelli, Arsalan Mousavian, Stephen Tyree, Stan Birchfield, Jonathan Tremblay, Justin Carpentier, Mathieu Aubry, Dieter Fox, and Josef Sivic. MegaPose: 6D

- Pose Estimation of Novel Objects via Render & Compare. In CoRL. 2
- [10] Taeyeop Lee, Bowen Wen, Minjun Kang, Gyuree Kang, In So Kweon, and Kuk-Jin Yoon. Any6d: Model-free 6d pose estimation of novel objects. The 2025 IEEE/CVF Computer Vision and Pattern Recognition Conference, 2025. 2
- [11] Haitao Lin, Zichang Liu, Chilam Cheang, Yanwei Fu, Guodong Guo, and Xiangyang Xue. Sar-net: Shape alignment and recovery network for category-level 6d object pose and size estimation. CVPR, 2022. 5
- [12] Jiehong Lin, Zewei Wei, Yabin Zhang, and Kui Jia. Vinet: Boosting category-level 6d object pose estimation via learning decoupled rotations on the spherical representations. *ICCV*, 2023. 5
- [13] Jiehong Lin, Lihua Liu, Dekun Lu, and Kui Jia. Sam-6d: Segment anything model meets zero-shot 6d object pose estimation. The 2024 The IEEE / CVF Computer Vision and Pattern Recognition Conference (CVPR), 2024. 2
- [14] Xiao Lin, Wenfei Yang, Yuan Gao, and Tianzhu Zhang. Instance-adaptive and geometric-aware keypoint learning for category-level 6d object pose estimation. In *Proceedings of* the IEEE/CVF Conference on Computer Vision and Pattern Recognition, pages 21040–21049, 2024. 5
- [15] Yuan Liu, Yilin Wen, Sida Peng, Cheng Lin, Xiaoxiao Long, Taku Komura, and Wenping Wang. Gen6d: Generalizable model-free 6-dof object pose estimation from rgb images. In ECCV, 2022. 2
- [16] Maxime Oquab, Timothée Darcet, Theo Moutakanni, Huy V. Vo, Marc Szafraniec, Vasil Khalidov, Pierre Fernandez, Daniel Haziza, Francisco Massa, Alaaeldin El-Nouby, Russell Howes, Po-Yao Huang, Hu Xu, Vasu Sharma, Shang-Wen Li, Wojciech Galuba, Mike Rabbat, Mido Assran, Nicolas Ballas, Gabriel Synnaeve, Ishan Misra, Herve Jegou, Julien Mairal, Patrick Labatut, Armand Joulin, and Piotr Bojanowski. Dinov2: Learning robust visual features without supervision, 2023. 2
- [17] Kiru Park, Timothy Patten, and Markus Vincze. Pix2pose: Pixel-wise coordinate regression of objects for 6d pose estimation. *ICCV*, 2019. 2
- [18] Sida Peng, Yuan Liu, Qixing Huang, Hujun Bao, and Xi-aowei Zhou. Pvnet: Pixel-wise voting network for 6dof pose estimation. CVPR, 2019.
- [19] Jiaming Sun, Zihao Wang, Siyu Zhang, Xingyi He, Hongcheng Zhao, Guofeng Zhang, and Xiaowei Zhou. OnePose: One-shot object pose estimation without CAD models. CVPR, 2022. 2
- [20] He Wang, Srinath Sridhar, Jingwei Huang, Julien Valentin, Shuran Song, and Leonidas J. Guibas. Normalized object coordinate space for category-level 6d object pose and size estimation. CVPR. 2019. 5
- [21] Y. You, W. He, J. Liu, H. Xiong, W. Wang, and C. Lu. Cppf++: Uncertainty-aware sim2real object pose estimation by vote aggregation. *IEEE Transactions on Pattern Analysis and Machine Intelligence*, 2024. 2, 5, 6
- [22] Linfang Zheng, Chen Wang, Yinghan Sun, Esha Dasgupta, Hua Chen, Ales Leonardis, Wei Zhang, and Hyung Jin Chang. Hs-pose: Hybrid scope feature extraction for category-level object pose estimation. CVPR, 2023. 5, 6